

Room-temperature current-voltage characteristics in AlAs-GaAs-AlAs double-barrier structures: Calculations using a bond-orbital model

Jiann-Shing Shyu

Physics and Chemistry Department, Chinese Military Academy, Feng-Shan, Kaohsiung, Taiwan, Republic of China

Jih-Chen Chiang

Department of Physics, National Sun Yat-sen University, Kaohsiung, Taiwan, Republic of China

(Received 19 October 1998; revised manuscript received 5 February 1999)

This paper reports the current-voltage characteristics of the AlAs-GaAs-AlAs double-barrier structures (DBS's) grown along the [001] and [111] directions at room temperature, within a fourth-neighbor bond-orbital model. We demonstrate that at room temperature the resonant-tunneling current is dominated by the L -valley electrons instead of Γ -valley electrons for an AlAs-GaAs-AlAs DBS with barrier widths of ~ 3 nm or more. We also demonstrate that at room temperature not only the peak current but also the peak-to-valley ratio can be significantly improved by orienting the materials along the [111] direction, due to the Γ - and L -point orientation effects. [S0163-1829(99)03727-3]

I. INTRODUCTION

The AlAs/GaAs material systems have been investigated intensively for potential device applications of resonant-tunneling phenomena.¹⁻³ Most of studies to date of AlAs/GaAs resonant-tunneling devices have considered materials grown along the [001] direction, that is, on substrates with the [001] crystal orientation. Recently, Luo *et al.*³ reported that a [111]-oriented AlAs-GaAs-AlAs double-barrier structure (DBS) consisting of 2.8 nm barriers and an 8 nm well shows a significant improvement in the peak-to-valley ratio (PVR) at both 77 K and room temperature, compared to the [001]-oriented DBS's with similar well and barrier layers. The above phenomenon was attributed to the increased effective mass of the X minima that contribute to the inelastic Γ - X - Γ tunneling current,³ i.e., the X -point orientation effect. This orientation effect is clearly very important, since the inelastic (and elastic) Γ - X - Γ tunneling may give dominant contribution to the valley current at low temperatures.⁴⁻⁷ Recently, we found that not only the Γ electrons but also the L electrons may give dominant contributions to the tunneling current at room temperature.⁸ Thus, to understand why the [111]-oriented DBS is superior to the [001]-oriented DBS at room temperature, we calculate the current-voltage (J - V) characteristics at room temperature for the [001]- and [111]-oriented AlAs-GaAs-AlAs DBS's, and compare our results with those as reported in Ref. 3. We find that at room temperature not only the peak current but also the PVR can be significantly improved by orienting the materials along the [111] direction, due to the Γ -point and L -point orientation effects.

To study the resonant-tunneling characteristics of the AlAs-GaAs-AlAs DBS's at room temperature, we develop a five-band fourth-neighbor bond-orbital model (FBO). In this paper, we shall demonstrate that this model is a very good model for studying the resonant-tunneling characteristics of the AlAs-GaAs-AlAs DBS at room temperature, since it can reproduce very accurate lowest conduction-band structure near the Γ and L points. The unpublished four-band FBO

model⁸ (TBO is a misprint in Ref. 8.) is also a good and efficient model for calculating the J - V characteristics of the AlAs-GaAs-AlAs DBS at room temperature; however, it can not very accurately describe the AlAs light-hole band anisotropic behavior, which is very important for studying the Γ -point orientation effect. The theoretical calculations, which included only the elastic-tunneling current contributed from the Γ -valley electrons, may yield much smaller valley current than the experimental results and, therefore, extremely overestimate the PVR by about a factor of 100 or more at room temperature.⁹⁻¹¹ Even for those theoretical methods⁵⁻⁷ that take into account both elastic Γ - Γ - Γ and Γ - X - Γ tunneling currents, as we know, they may also yield much smaller valley current than the experimental results at room temperature. In this paper, we shall also illustrate the physical origin for the appearance of a shoulder structure in the J - V characteristics of the [001]-oriented DBS as shown in Fig. 2(c) of Ref. 3; we shall also explain why the best room-temperature PVR in the pseudomorphic In_{0.53}Ga_{0.47}As/AlAs/InAs diodes is much better than that in the GaAs/AlAs diodes,^{2,12} and why the negative differential resistance may not be observed at room temperature in an AlAs-GaAs-AlAs DBS with thick AlAs barriers (e.g., >3 nm).⁹

II. THEORETICAL METHOD

To calculate the J - V characteristics of the AlAs-GaAs-AlAs DBS's grown along [001] and [111] directions at room temperature, we use the five-band FBO model that describes the lowest conduction band and valence bands in terms of linear combination of antibonding and bonding orbitals. One s -like antibonding orbital, one s -like bonding orbital, and 3 p -like bonding orbitals per unit site (i.e., per bulk unit cell) for a face-centered cubic lattice are used. The Hamiltonian $H_0(\mathbf{k})$ for a bulk semiconductor is given in the Appendix. It should be noted that in the Hamiltonian $H_0(\mathbf{k})$, the third-neighbor interactions are not taken into account. This will be discussed later in the Discussions section.

In our model, a DBS can be viewed as a stack of infinite number of diatomic layers along the growth direction. A Bloch sum with in-plane wave vector \mathbf{k}_{\parallel} of bond orbital within the l th diatomic layer is denoted by $|l\alpha, \mathbf{k}_{\parallel}\rangle$, where $\alpha = s', s, x, y, z$ denotes the symmetry type of bond orbital. We divide the DBS into three regions: a semi-infinite bulk-like region on the left, a semi-infinite bulklike region on the right and a central double-barrier region. Since \mathbf{k}_{\parallel} is a good quantum number, the eigenstate of the entire structure may be written as $|\Psi\rangle = \sum_{l\alpha} F_{l\alpha} |l\alpha, \mathbf{k}_{\parallel}\rangle$. Since the FBO model is a second-layer orbital model¹³ for [001]- and [111]-oriented DBS's the Schrödinger equation $(H - E)|\Psi\rangle = 0$ can be written in the layer-orbital basis as

$$\begin{aligned} & \bar{H}_{l,l-2}F_{l-2} + \bar{H}_{l,l-1}F_{l-1} + \bar{H}_{l,l}F_l + \bar{H}_{l,l+1}F_{l+1} + \bar{H}_{l,l+2}F_{l+2} \\ & = 0, \end{aligned} \quad (1)$$

where $\bar{H}_{l,l}$ and $\bar{H}_{l,l'}$ are 5×5 matrices and they are truncated at a fourth-neighbor distance. F_l denotes a five-dimensional column vector whose components are $F_{l\alpha}$. The elements of matrix $\bar{H}_{l,l'}$ are $(\bar{H}_{l,l'})_{\alpha\alpha'} = \langle l\alpha, \mathbf{k}_{\parallel} | H - E | l\alpha', \mathbf{k}_{\parallel} \rangle$.

The boundary conditions for this problem are such that there is a known incoming plane wave from the left, unknown bulk states transmitting or decaying to the right, and unknown bulk states reflecting or decaying to the left. A bulk state associated with energy E and complex vector k_3 may be described by $|k_3\rangle = \sum_{l\alpha} B_{l\alpha} |l\alpha, \mathbf{k}_{\parallel}\rangle$, where the tight-binding coefficients $B_{l\alpha}$ must obey the relation $B_l = e^{ik_s a'} B_{l-1}$, where a' is the distance between two adjacent diatomic layers. Using this relation and Eq. (1), the complex wave vector and their associated bulk states can be obtained by solving the related eigenvalue problem for the transfer matrix.¹⁴

For a given incoming plane wave (denoted by i) incident from the left, the wavefunctions in the left (L) and right (R) bulk regions can be expressed in terms of the bulk states:

$$|\Psi; L\rangle = I_i |k_{3,i}; L\rangle + \sum_{j \in \mathcal{L}} r_j |k_{3,j}; L\rangle, \quad (2)$$

$$|\Psi; R\rangle = \sum_{j \in \mathcal{R}} t_j |k_{3,j}; R\rangle, \quad (3)$$

where \mathcal{L} and \mathcal{R} denote the sets of outgoing waves that propagate (or decay) to the left and right, respectively. The transmission and reflection amplitudes t_j and r_j can be solved by substituting Eqs. (2) and (3) into Eq. (1) and matching the boundary conditions. An efficient numerical method to solve the problem can be found in Ref. 11 for a bond-orbital model with nearest-neighbor interactions. Here the procedure used

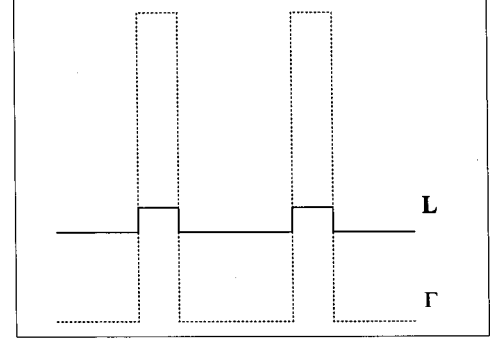


FIG. 1. Schematic potential profiles for an AlAs-GaAs-AlAs DBS.

is similar, but complicated by the existence of fourth-neighbor (or second-layer) interactions.¹³ The transmission coefficient for an incident plane-wave (labeled i) now can be found by the expression

$$T(E, \mathbf{k}_{\parallel}) = \sum_{j=1}^{N_p} |t_j(E, \mathbf{k}_{\parallel})|^2 \frac{|v_j(E, \mathbf{k}_{\parallel}; R)|}{|v_i(E, \mathbf{k}_{\parallel}; L)|}, \quad (4)$$

where N_p is the total number of transmitted bulk plane-wave states, and $v_i(E, \mathbf{k}_{\parallel}; R)$ and $v_j(E, \mathbf{k}_{\parallel}; L)$ are the group velocities of the incident and transmitted bulk propagating states. The tunneling current density is related to the transmission coefficient by¹⁵

$$J = \frac{e}{4\pi^3 \hbar} \int T(E, \mathbf{k}_{\parallel}) [f(E) - f(E + eV)] dE_{\perp} d^2 \mathbf{k}_{\parallel}, \quad (5)$$

where V is the voltage difference across the DBS, $f(E)$ is the Fermi distribution of the incident electron population.

III. RESULTS

For an AlAs-GaAs-AlAs DBS, not only the Γ point but also the L -point profiles show a double-barrier configuration (see Fig. 1); and the L -point offset between AlAs and GaAs is about 0.1 eV while the Γ -point offset between AlAs and GaAs is about 1 eV. The [001]-oriented AlAs-GaAs-AlAs DBS studied in this paper (i.e., the [001]-oriented sample) consists of 2.8 nm (10 diatomic layer) barriers and a 7.9 nm (28 diatomic layer) well; and the [111]-oriented DBS studied here (i.e., the [111]-oriented sample) consists of 2.9 nm (9 diatomic layer) barriers and a 7.8 nm (24 diatomic layer) well. For convenience, in this paper we denote the tunneling current densities due to the incident L -valley electrons and Γ -valley electrons as the J_L and J_{Γ} , respectively. We also

TABLE I. Interaction parameters for GaAs and AlAs. All parameters are in units of eV.

	$E_{s'}$	E_p	$U_{s's'}$	$U_{s'x}$	U_{zz}	U_{xx}	U_{xy}	$V_{s's'}$	$V_{s'x}$	W_{sx}
GaAs	2.148	-3.048	-0.054	0.443	-0.069	0.419	0.450	0.030	-0.349	-0.1
AlAs	2.822	-2.723	-0.020	0.340	-0.074	0.368	0.415	0.071	-0.266	0.1
	$W_{s'x}$	W_{xx}	W_{zz}	E_s	U_{ss}	V_{ss}	W_{ss}	U_{sx}	$W_{s's'}$	
GaAs	0.070	-0.039	0.070	-10.3	-0.170	0.008	-0.02	0.210	-0.014	
AlAs	0.094	-0.053	0.124	-10.0	-0.138	0.004	-0.02	0.200	-0.003	

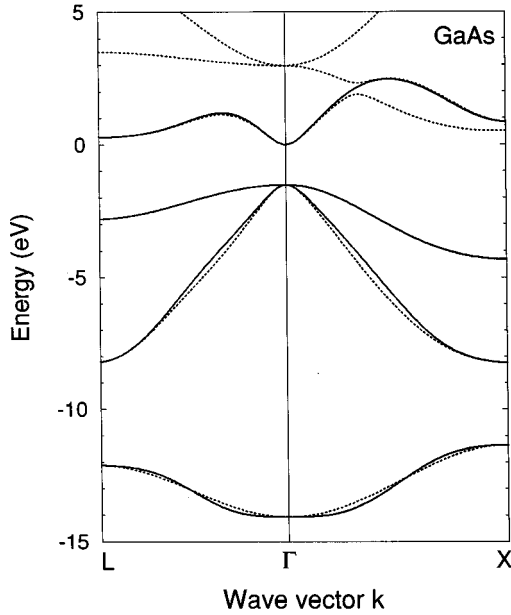


FIG. 2. Real band structures of bulk GaAs calculated from five-band FBO model (solid lines) and eight-band FBO model (dotted lines).

use the conduction-band minimum energy of bulk GaAs (denoted E_{Γ}^{GaAs}) as our reference energy. The interaction parameters for AIAs and GaAs materials are listed in Table I.

In Fig. 2, the solid lines represent the real band structures of bulk GaAs calculated using the five-band FBO model. It is clear that this model can reproduce fairly accurate valence band structures in the whole Brillouin zone, and very accurate lowest conduction-band structure near the Γ and L points. This indicates that the tunneling currents contributed from the Γ -valley and L -valley electrons are included in this model for the calculations of the J - V characteristics. However, the Γ - X - Γ tunneling⁵ cannot be included in the calculations, since the X -point conduction-band minima are not accurately described by the five-band FBO model. Fortunately, for the present DBS's, the Γ - X - Γ tunneling does not give very important contribution to the J - V characteristics at room temperature and, therefore, the five-band FBO model is a good approximation for calculating the J - V characteristics at room temperature. This will be further discussed later. It may be worth pointing out that, as shown by the dotted lines in Fig. 2, the eight-band FBO model (which is unpublished) can reproduce a very accurate lowest conduction band in the whole Brillouin zone; however, it takes extremely long computer time for calculating the J - V characteristics. The effective masses in GaAs are taken to be $m_{\Gamma}^* = 0.065m_0$, $m_{L,l}^* = 1.9m_0$, $m_{L,t}^* = 0.075m_0$, and $m_{lh}^{001} = 0.076m_0$.¹⁶ Here m_{Γ}^* is the Γ valley electron effective mass; $m_{L,l}^*$ and $m_{L,t}^*$ are the longitudinal and transverse L -valley electron effective masses, respectively; and m_{lh}^{001} is the light-hole band effective mass in [001] direction.

In addition to the real band structures of bulk AIAs (solid lines), the purely imaginary conduction to light-hole band (labeled C-LH), which connects the conduction-band minimum with the light-hole band maximum, are also shown by dotted lines in Fig. 3. Evidently, the AIAs C-LH band exhib-

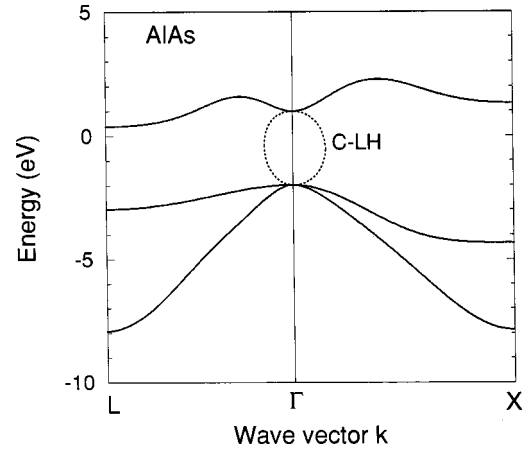


FIG. 3. Complex band structures of bulk AIAs.

its an anisotropic behavior: For a fixed energy, the imaginary k of AIAs C-LH band in [111] direction is clearly smaller than that in [001] direction. The C-LH band exhibits an anisotropic behavior because its state is a mixing state of the isotropic conduction band and anisotropic light-hole band. The C-LH band anisotropy is strong in AIAs since in AIAs m_{lh}^{111} is much smaller than m_{lh}^{001} . The effective masses in AIAs are taken to be $m_{\Gamma}^* = 0.15m_0$, $m_{L,l}^* = 1.9m_0$, $m_{L,t}^* = 0.096m_0$, $m_{lh}^{001} = 0.15m_0$, and $m_{lh}^{111} = 0.1m_0$.¹⁶

Figure 4 shows the calculated transmission coefficients (T) caused by the incident Γ -valley electrons with $\mathbf{k}_{\parallel} = (0,0)$, for the [001]-oriented (solid lines) and [111]-oriented (dotted lines) samples. The resonance-peak structures are labeled as Γ_n ($n = 1, 2, \dots$), where Γ_n represents n th Γ -point quasibound state. It is clear that for each Γ (Γ_1 or Γ_2) resonance-peak structure, the integrated transmission coefficient (transmission coefficient integrated over the incident electron energies) of the [111]-oriented sample is significantly larger than that of the [001]-oriented sample, due to the AIAs C-LH band anisotropic behavior. This implies that for an AIAs-GaAs-AIAs DBS, the resonant-tunneling current caused by the incident electrons derived from the Γ valley can be significantly improved by orienting the growth direction from [001] to [111]. We refer to this phenomenon as the AIAs C-LH band anisotropic effect, or the Γ -point orientation effect.

Figure 5 shows the calculated transmission coefficients

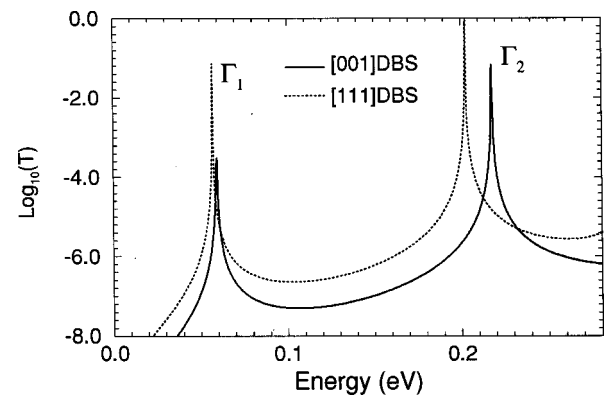


FIG. 4. Calculated transmission coefficients (T) caused by the incident Γ -valley electrons with $\mathbf{k}_{\parallel} = (0,0)$.

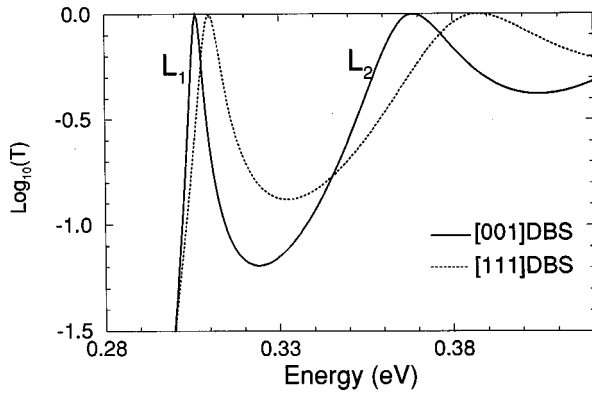


FIG. 5. Calculated transmission coefficients caused by the incident electrons derived from the L -valley located at $\mathbf{k} = (\pi/a)(1,1,-1)$.

caused by the incident electrons derived from the L valley located at $\mathbf{k} = (\pi/a)(1,1,-1)$. The solid line is obtained with $\mathbf{k}_{\parallel} = (\pi/a)(0.5, 0.5)$ for the [001]-oriented sample, while the dotted line is obtained with $\mathbf{k}_{\parallel} = (\pi/a)(2/\sqrt{6}, 0)$ for the [111]-oriented sample (Please refer to Fig. 1 of Ref. 13). The resonance-peak structures are labeled as L_n ($n = 1, 2, \dots$), where L_n represents n th L -point quasibound state. Please note that, due to symmetry, the transmission spectra associated with three other equivalent L valleys in the [001]-oriented sample [which are located at $\mathbf{k} = (\pi/a)(-1, 1, 1)$, $(\pi/a)(1, -1, 1)$, and $(\pi/a)(1, 1, 1)$] are identical to the solid curve, and those associated with two other equivalent L valleys in the [111]-oriented sample [which are centered at $\mathbf{k} = (\pi/a)(-1, 1, 1)$ and $(\pi/a)(1, -1, 1)$] are identical to the dotted curve shown here. As for the transmission probability of the incident electrons derived from the L valley located at $\mathbf{k} = (\pi/a)(1, 1, 1)$ in the [111]-oriented sample, it is very weak since the tunneling effective mass is as heavy as $1.9m_0$. Thus, we conclude that in a [111]-oriented AlAs-GaAs-AlAs DBS only three L valleys, instead of four in a [001]-oriented DBS, give significant contribution to the tunneling current.

In Fig. 5, it is seen that in each ([001]- or [111]-oriented) sample, the integrated transmission coefficient for the L_2 resonance-peak structure is much larger than that for the L_1 resonance-peak structure. This means that in each sample, the J_L is dominated by the resonant-tunneling via the L_2 quasibound state. It is also seen that the integrated transmission coefficient for the L_2 resonance-peak structure in the [111]-oriented sample is larger but not much larger than (is about 1.4 times as large as) that in the [001]-oriented sample. This indicates that the L valley located at $\mathbf{k} = (\pi/a)(1, 1, -1)$ in the [111]-oriented sample provides stronger but not much stronger tunneling current than that in the [001]-oriented sample. Moreover, in a [111]-oriented DBS only three L valleys give significant contribution to the tunneling current. Thus, we expect that the second peak current density (i.e., the peak current density due to resonant-tunneling via the L_2) of the J_L in the [111]-oriented sample should be larger, but only slightly larger than that in the [001]-oriented sample. We refer to this phenomenon as the L -point orientation effect. Note that the integrated transmission coefficient for each L (L_1 or L_2) resonance-peak structure in the [111]-

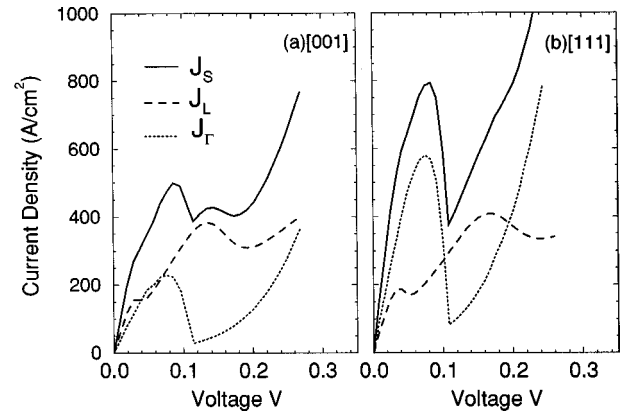


FIG. 6. The current-voltage characteristics of (a) the [001]-oriented and (b) the [111]-oriented AlAs-GaAs-AlAs samples at 300 K. Here, V denotes the voltage across the DBS.

oriented sample is larger than that in the [001]-oriented sample simply because the tunneling effective mass in a [111]-oriented DBS is smaller than that in a [001]-oriented DBS.

Figure 6 shows the J - V characteristics of (a) the [001]-oriented and (b) the [111]-oriented AlAs-GaAs-AlAs samples at 300 K. The dashed line stands for the J_L component; the dotted line represents the J_{Γ} component; and the solid line is the J_S , i.e., the sum of the two contributions. The chemical potential used here is 0.04 eV. In Fig. 6(a), it is clear that the solid curve exhibits a double-peak structure in which the first one is stronger than the second one. The stronger one is caused by the tunneling via the Γ_1 , while the weaker one is caused by the tunneling via the L_2 (please refer to Figs. 4–5). We believe that the weaker one may be replaced by a shoulder structure as shown in Fig. 2 of Ref. 3, if inelastic tunneling effects are also taken into account in our calculations. The weaker peak structure (or the shoulder structure) cannot be observed in the [111]-oriented sample [see also Fig. 2(a) of Ref. 3], since the background current due to resonant tunneling via the Γ_2 increases very rapidly near the second peak voltage of the J_L component.

In Fig. 6, it is found that the peak current density of the J_S in the [111]-oriented sample is significantly larger than that in the [001]-oriented sample, even though the peak current density contributed from the J_L component in the [111]-oriented sample is smaller (about 90 \AA/cm^2 smaller) than that in the [001]-oriented sample (see the dashed lines). This clearly results from the Γ -point orientation effect, since the peak current density of the J_{Γ} component in the [111]-oriented sample is much larger (about 390 \AA/cm^2 larger) than that in the [001]-oriented sample (see the dotted lines). It is also found that in each sample ([001]-oriented or [111]-oriented sample), the valley current density of the J_S is nearly the same as the second peak current density of the J_L component. This can be understood by the fact that in each sample, the valley current density of the J_S is dominated by the J_L component and the second peak voltage of the J_L component is very close to the valley voltage of the J_{Γ} component. In addition, the second peak current density of the J_L component (i.e., peak current density due to tunneling via the L_2) in the [111]-oriented sample is only slightly larger than that in the [001]-oriented sample (see dashed lines), as a

result of the L -point orientation effect. Thus, due to the L -point orientation effect, the valley current density of the J_S in the $[111]$ -oriented sample should be approximately equal to that in the $[001]$ -oriented sample. As expected, in Fig. 6 we do find that the valley current of the J_S in the $[111]$ -oriented sample is about the same as that in the $[001]$ -oriented sample. From the above discussions, we conclude that at room temperature not only the peak current density but also the PVR in a $[111]$ -oriented AlAs-GaAs-AlAs DBS are better than those in a $[001]$ -oriented DBS with similar well and barrier layers, due to the Γ -point and L -point orientation effects. This conclusion is confirmed by the fact that our PVR's (2.1 for $[111]$ - and 1.3 for $[001]$ -oriented DBS) are in very good agreement with the experimental results (1.8 for $[111]$ - and 1.2 for $[001]$ -oriented DBS) as reported in Fig. 2 of Ref. 3. This satisfactory agreement also indicates that the elastic L - L - L and Γ - Γ - Γ tunneling currents give dominant contributions to the J - V characteristics for the present DBS's at room temperature. Certainly, the satisfactory agreement in PVR's also implies that the five-band FBO elastic-tunneling model, which can very accurately describe the lowest conduction-band structure near both the Γ and L points, is a very good approximation for studying the resonant-tunneling characteristics of the AlAs-GaAs-AlAs DBS at room temperature.

IV. DISCUSSIONS

In Ref. 8, we predicted that, due to L -electron effect, the tunneling current at room temperature may be dominated by the L electrons instead of Γ electrons, if the AlAs barriers become thick enough (e.g., >3 nm). As expected, in Fig. 6 we do find that the second peak current density of the J_L [denoted $J_p(L_2)$] is significantly larger than the first peak current density of the J_Γ [denoted $J_p(\Gamma_1)$] in the J - V characteristics of the $[001]$ -oriented sample (barrier width: 2.8 nm). This clearly confirms our prediction reported in Ref. 8. To understand why the resonant-tunneling current at room temperature is indeed dominated by the L electrons for an AlAs-GaAs-AlAs DBS with thick barrier widths (>3 nm), we shall estimate the ratio of $J_p(L_2)$ to $J_p(\Gamma_1)$ for the $[001]$ -oriented sample. It is known that the current density J is not only related to integrated transmission coefficient (ITC) but also related to the two-dimensional density of states (DOS) and thermal occupation $f(E)$ [please refer to Eq. (5)]. Thus, $J_p(L_2)/J_p(\Gamma_1)$ at room temperature can be easily estimated by⁸

$$\begin{aligned} \frac{J_p(L_2)}{J_p(\Gamma_1)} &\approx \frac{e^{-[E_L^{\text{GaAs}} - \mu(T)]/kT}}{1} \times \frac{(\text{DOS})_L}{(\text{DOS})_\Gamma} \times \frac{(\text{ITC})_L}{(\text{ITC})_\Gamma} \\ &\approx \frac{e^{-(290-40)/30}}{1} \times \frac{20}{1} \times \frac{300}{1} > 1, \end{aligned} \quad (6)$$

where the GaAs conduction-band minimum energy at L point (E_L^{GaAs}) is about 290 meV,¹⁶ and the chemical potential $\mu(T)$ are assumed to be 40 meV. Clearly, at room temperature the L electrons are very important in AlAs-GaAs-AlAs DBS system, because $(\text{DOS})_L \gg (\text{DOS})_\Gamma$, $(\text{ITC})_L \gg (\text{ITC})_\Gamma$, and E_L^{GaAs} is only about 0.29 eV higher than E_Γ^{GaAs} . Moreover, $(\text{ITC})_L/(\text{ITC})_\Gamma$ increases rapidly with in-

creasing barrier widths, because the L -point barrier height ($\Delta E_L \approx 0.1$ eV) is much smaller than the Γ -point barrier height ($\Delta E_\Gamma \approx 1$ eV). Thus, we conclude that for an AlAs-GaAs-AlAs DBS with thick barrier widths (>3 nm), the resonant-tunneling current is indeed dominated by the elastic L - L - L tunneling instead of the Γ - Γ - Γ tunneling at room temperature. This explains why the NDR may not be observed at room temperature in an AlAs-GaAs-AlAs DBS with thick AlAs barriers (>3 nm).⁹ Note that in AlAs-GaAs-AlAs DBS system, the L -valley electrons have significant contribution to the valley current at room temperature, mainly because the L -valley minimum is only about 0.29 eV (see Ref. 16) higher than the Γ -valley minimum in GaAs bulk regions. This explains why the best room-temperature PVR in the GaAs/AlAs diodes (3.5) is much smaller than that in the pseudomorphic $\text{In}_{0.53}\text{Ga}_{0.47}\text{As}/\text{AlAs}/\text{InAs}$ diodes (30),^{2,12} since in $\text{In}_{0.53}\text{Ga}_{0.47}\text{As}$ the L -valley minimum is about 0.7 eV higher than the Γ -valley minimum.

From the above discussions, we understand that $f(E)$, DOS, and ITC are three dominant factors for calculating the J - V characteristics at room temperature. Our FBO model reproduces very accurate band structures near the Γ and L points and, therefore, provides very accurate $f(E_\alpha)$, $(\text{DOS})_\alpha$, and $(\text{ITC})_\alpha$ ($\alpha=L, \Gamma$). This explains why our model works so well with experimental results in AlAs-GaAs-AlAs DBS system at room temperature. In fact, bond-orbital models have been demonstrated to be a very good method for studying the band-structure effects (e.g., anisotropic and nonparabolic effects of the lowest conduction band).^{13,17-19} In our recently published paper, as shown in Fig. 3 of Ref. 17, we calculate the J - V characteristics using the second-neighbor sp^3 bond-orbital (SBO), nearest-neighbor sp^3 bond-orbital (NBO), and two-band $k \cdot p$ models. In Fig. 3 of Ref. 17, it is clear that the three J - V curves are quite similar. This indicates that all three models are good models for studying the intravalley tunneling characteristics. In Fig. 3 of Ref. 17, it is also seen that the J - V curve obtained from the SBO model is better than those obtained from the NBO and $k \cdot p$ models, because the band structures reproduced by the SBO model are better than those obtained from the NBO and the $k \cdot p$ models (please see Fig. 1 in Ref. 17). Evidently, the four-band semiempirical SBO model is a very good band-structure model for studying the Γ -point intravalley tunneling characteristics in AlSb-InAs-AlSb DBS's. However, it is not a very good band-structure model for studying the intravalley tunneling characteristics (Γ - Γ - Γ and L - L - L) in AlAs-GaAs-AlAs DBS's, since it cannot reproduce very good band structures near the L points. Due to this reason, by adding some small fourth-neighbor interactions to the SBO model, we develop a FBO model. Clearly, the FBO model is a very good band-structure model for studying the intravalley tunneling characteristics (Γ - Γ - Γ and L - L - L) in AlAs-GaAs-AlAs DBS's, since it can reproduce very good band structures near the Γ and L points. The five-band FBO model is slightly better than the four-band FBO model since, as mentioned above, the five-band FBO model can describe the light-hole band anisotropy more accurately than the four-band FBO model.

It should be noted that the third-neighbor interactions are not included in our FBO model. Now, we shall use $H_{s's'}$ as an example to explain why the third-neighbor interactions

can be removed in our present calculations. Note that $H_{s's'}$ is the most important matrix element for reproducing accurate lowest conduction-band structure along the Γ - L direction. When the third-neighbor interactions are also included in our calculations, $H_{s's'}$ in the Appendix can be written as

$$H_{s's'} = E_{s'} + U_{s's'}T_s + V_{s's'}C_s + Q_{s's'}D_s + W_{s's'}R_s. \quad (7)$$

Here, $E_{s'}$ is the on-site orbital energy for the s -like antibond orbital; $U_{s's'}$ denotes the nearest-neighbor interaction between an s -like antibond orbital at the origin and an s -like antibond orbital at $(\frac{1}{2}, \frac{1}{2}, 0)a$; $V_{s's'}$ denotes the second-neighbor interaction between an s -like antibond orbital at the origin and an s -like antibond orbital at $(1, 0, 0)a$; $Q_{s's'}$ represents the third-neighbor interaction between an s -like antibond orbital at the origin and an s -like antibond orbital at $(\frac{1}{2}, \frac{1}{2}, 1)a$; and $W_{s's'}$ represents the fourth-neighbor interaction between an s -like antibond orbital at the origin and an s -like antibond orbital at $(1, 1, 0)a$. The k -dependent parameters are

$$T_s = 4[\cos(k_x a/2)\cos(k_y a/2) + \cos(k_y a/2)\cos(k_z a/2) + \cos(k_z a/2)\cos(k_x a/2)],$$

$$C_s = 2[\cos(k_x a) + \cos(k_y a) + \cos(k_z a)],$$

$$D_s = 8[\cos(k_x a)\cos(k_y a/2)\cos(k_z a/2) + \cos(k_y a)\cos(k_x a/2)\cos(k_z a/2) + \cos(k_z a)\cos(k_x a/2)\cos(k_y a/2)],$$

$$R_s = 4[\cos(k_x a)\cos(k_y a) + \cos(k_y a)\cos(k_z a) + \cos(k_z a)\cos(k_x a)].$$

It is clear that at L points, $T_s = 0$, $C_s = -6$, $D_s = 0$, and $R_s = 12$. This implies that the second- and fourth-neighbor interactions are much more important than the first- and third-neighbor interactions near the L points, since $U_{s's'}T_s \approx 0$ and $Q_{s's'}D_s \approx 0$. As a matter of fact, the fourth-neighbor interactions may be as important as the second-neighbor interactions near the L points, since $C_s = -6$ and $R_s = 12$. In addition, due to the fact that $U_{s's'}$ and $V_{s's'}$ are larger than $Q_{s's'}$ and $W_{s's'}$, the first- and second-neighbor interactions are much more important than the third- and fourth-neighbor interactions near the Γ point. Thus, we conclude that the third-neighbor interactions can be removed in our calculations, since in our present paper we concentrate on the studies of the Γ -electron and L -electron effects. Clearly, we did not assume that $Q_{s's'} = 0$ (i.e., $1\text{st} > 2\text{nd} > 4\text{th} > 3\text{rd} = 0$); however, due to symmetry effect, $Q_{s's'}D_s$ does equal 0 at L points. In fact, even the third-neighbor interactions are also included in our calculations, same results must be obtained; however, the calculations will become much more complicated.

Generally speaking, any model (e.g., five-band bond-orbital, eight-band tight-binding, effective mass, or two-band $k \cdot p$) can be a good band-structure model for studying the α - α - α ($\alpha = \Gamma, L, \text{ or } X$) intravalley tunneling characteristics, if it can reproduce good band structures near the α point.

Among bond-orbital, tight-binding, effective-mass, and $k \cdot p$ methods, bond orbital, and tight binding are the best two methods for studying the band-structure effects. We choose a bond-orbital model because it is much simpler and much more efficient than a tight-binding model. It may be worth pointing out that a five-band or even an eight-band bond-orbital model may not be a good model for studying the intervalley tunneling (e.g., Γ - X - Γ , X - Γ - X , and Γ - L - Γ) characteristics in semiconductor DBS's, since it may not be able to describe the intervalley mixing effects very accurately. In order to describe the intervalley mixing effects very accurately, a more realistic but complicated band-structure model (e.g., $s^2d^{10}p^6$ tight-binding model)²⁰ may be needed; however, the calculations require extremely long computer time. Please note that for intervalley tunneling, a band-structure model cannot provide an accurate ITC, if it cannot accurately describe the intervalley mixing effects.

V. CONCLUSIONS

In summary, we develop a five-band fourth-neighbor bond-orbital model to study the current-voltage characteristics of the AlAs-GaAs-AlAs DBS's grown along the $[001]$ and $[111]$ directions at room temperature. We demonstrate that at room temperature the resonant-tunneling current is dominated by the L -valley electrons instead of Γ -valley electrons for an AlAs-GaAs-AlAs DBS with barrier widths of ~ 3 nm or more. We also demonstrate that at room temperature not only the peak current but also the peak-to-valley ratio can be significantly improved by orienting the materials along the $[111]$ direction, due to the Γ - and L -point orientation effects. In this paper, we also explain why the best room-temperature PVR in the pseudomorphic $\text{In}_{0.53}\text{Ga}_{0.47}\text{As}/\text{AlAs}/\text{InAs}$ diodes is much better than that in the GaAs/AlAs diodes,^{2,12} explain why the negative differential resistance may not be observed at room temperature in an AlAs-GaAs-AlAs DBS with thick AlAs barriers (e.g., > 3 nm),⁹ and explain why a shoulder structure appears in the J - V characteristics of the $[001]$ -oriented sample as shown in Fig. 2(c) of Ref. 3.

ACKNOWLEDGMENT

This work was supported in part by the National Science Council of the Republic of China.

APPENDIX

The tight-binding Hamiltonian within the bond-orbital basis for a bulk semiconductor with an fcc lattice can be written as

$$H_0(\mathbf{k}) = \begin{bmatrix} H_{s's'} & H_{s'x} & H_{s'y} & H_{s'z} & 0 \\ H_{s'x}^* & H_{xx} & H_{xy} & H_{xz} & H_{sx}^* \\ H_{s'y}^* & H_{xy}^* & H_{yy} & H_{yz} & H_{sy}^* \\ H_{s'z}^* & H_{xz}^* & H_{yz}^* & H_{zz} & H_{sz}^* \\ 0 & H_{sx} & H_{sy} & H_{sz} & H_{ss} \end{bmatrix}, \quad (\text{A1})$$

where

$$\begin{aligned}
H_{s't's'} &= E_{s'} + U_{s't's'}T_s + V_{s't's'}C_s + W_{s't's'}R_s, \\
H_{ss} &= E_s + U_{ss}T_s + V_{ss}C_s + W_{ss}R_s, \\
H_{s'\alpha} &= U_{s'x}T_\alpha + V_{s'x}S_\alpha + W_{s'x}R_\alpha \quad (\alpha = x, y, z), \\
H_{s\alpha} &= U_{sx}T_\alpha + W_{sx}R_\alpha \quad (\alpha = x, y, z), \\
H_{\alpha\alpha} &= E_p + U_{zz}T_s + (U_{xx} - U_{zz})T_\alpha + W_{zz}R_s \\
&\quad + (W_{xx} - W_{zz})R_\alpha \quad (\alpha = x, y, z), \\
H_{\alpha\beta} &= U_{xy}T_{\alpha\beta} \quad (\alpha = x, y, z; \beta = x, y, z; \alpha \neq \beta).
\end{aligned}$$

$E_{s'}$ is the on-site orbital energy for the s -like antibond orbital; E_s and E_p are the on-site orbital energy for the s - and p -like bond orbitals, respectively. $U_{\alpha\beta}$ ($\alpha\beta = s', s, x, y, z$) denotes the nearest-neighbor interaction between an α -like bond orbital at the origin and a β -like bond orbital at $(1,1,0)a/2$; $V_{\alpha\beta}$ ($\alpha\beta = s', s, x, y, z$) denotes the second-neighbor interaction between an α -like bond orbital at the origin and a β -like bond orbital at $(1,0,0)a$; and $W_{\alpha\beta}$ ($\alpha\beta = s', s, x, y, z$) represents the fourth-neighbor interaction between an α -like bond orbital at the origin and a β -like bond orbital at $(1,1,0)a$. We, thus, have 19 adjustable parameters. Please note that the third-neighbor interactions are not included in our FBO model, since they are not important for reproducing accurate L -point conduction-band minima. The k -dependent parameters in Eq. (A1) are

$$\begin{aligned}
T_x &= 4i \sin(k_x a/2) [\cos(k_y a/2) + \cos(k_z a/2)], \\
T_y &= 4i \sin(k_y a/2) [\cos(k_x a/2) + \cos(k_z a/2)], \\
T_z &= 4i \sin(k_z a/2) [\cos(k_x a/2) + \cos(k_y a/2)], \\
T_{xx} &= 4 \cos(k_x a/2) [\cos(k_y a/2) + \cos(k_z a/2)], \\
T_{yy} &= 4 \cos(k_y a/2) [\cos(k_x a/2) + \cos(k_z a/2)], \\
T_{zz} &= 4 \cos(k_z a/2) [\cos(k_x a/2) + \cos(k_y a/2)], \\
T_{xy} &= -4 \sin(k_x a/2) \sin(k_y a/2), \\
T_{xz} &= -4 \sin(k_x a/2) \sin(k_z a/2), \\
T_{yz} &= -4 \sin(k_y a/2) \sin(k_z a/2), \\
T_s &= \frac{1}{2}(T_{xx} + T_{yy} + T_{zz}),
\end{aligned}$$

$$\begin{aligned}
S_x &= 2i \sin(k_x a), \\
S_y &= 2i \sin(k_y a), \\
S_z &= 2i \sin(k_z a), \\
C_x &= 2 \cos(k_x a), \\
C_y &= 2 \cos(k_y a), \\
C_z &= 2 \cos(k_z a), \\
C_s &= C_x + C_y + C_z,
\end{aligned}$$

$$\begin{aligned}
R_x &= 4i \sin(k_x a) [\cos(k_y a) + \cos(k_z a)], \\
R_y &= 4i \sin(k_y a) [\cos(k_x a) + \cos(k_z a)], \\
R_z &= 4i \sin(k_z a) [\cos(k_x a) + \cos(k_y a)], \\
R_{xx} &= 4 \cos(k_x a) [\cos(k_y a) + \cos(k_z a)], \\
R_{yy} &= 4 \cos(k_y a) [\cos(k_x a) + \cos(k_z a)], \\
R_{zz} &= 4 \cos(k_z a) [\cos(k_x a) + \cos(k_y a)],
\end{aligned}$$

$$R_s = \frac{1}{2}(R_{xx} + R_{yy} + R_{zz}).$$

Along special directions (Γ - X and Γ - L) the 5×5 Hamiltonian can be diagonalized easily, and we obtain simple relations between the interaction parameters and the band energies:

$$\begin{aligned}
U_{ss} &= [E_s(\Gamma) - E_s(X)]/16, \\
U_{s't's'} &= [E_{s'}(\Gamma) - E_{s'}(X)]/16, \\
V_{ss} &= [E_s(\Gamma) - E_s(L) - 12U_{ss}]/12, \\
V_{s't's'} &= [E_{s'}(\Gamma) - E_{s'}(L) - 12U_{s't's'}]/12, \\
E_s &= E_s(\Gamma) - 12U_{ss} - 6V_{ss} - 12W_{ss}, \\
E_{s'} &= E_{s'}(\Gamma) - 12U_{s't's'} - 6V_{s't's'} - 12W_{s't's'}, \\
U_{xx} &= [E_x(\Gamma) - E_x^1(X)]/16, \\
U_{zz} &= [E_x(\Gamma) - E_x^2(X) - 8U_{xx}]/8, \\
U_{xy} &= [E_x^2(L) - E_x^1(L)]/12, \\
W_{zz} &= -[(\hbar^2/m_{hh}a^2) + U_{xx} + U_{zz} + 4W_{xx}]/4, \\
E_p &= E_x(\Gamma) - 4U_{zz} - 8U_{xx} - 4V_{zz} - 2V_{xx} - 4W_{zz} - 8W_{xx}, \\
(2U_{s't's'} + V_{s't's'} + 4W_{s't's'})^2 &= [E_{s'}(\Gamma) - E_x(\Gamma)][(\hbar^2/m_c a^2) \\
&\quad + 2U_{s't's'} + 2V_{s't's'} + 8W_{s't's'}]/8.
\end{aligned}$$

Here, m_Γ^* is the effective mass of the Γ -point conduction-band minimum and m_{hh}^{001} is the heavy-hole band effective mass in $[001]$ direction; $E_s(\Gamma)$, $E_s(X)$, and $E_s(L)$ are the energies of the s -like valence band at Γ , X , and L points, respectively; $E_{s'}(\Gamma)$, $E_{s'}(X)$, and $E_{s'}(L)$ are the energies of the s -like conduction band at Γ , X , and L points, respectively; $E_x^n(X)$ and $E_x^n(L)$ ($n = 1, 2$) are the energies of the n th p -like valence band at X and L points, respectively, where $E_x^1(\nu) > E_x^2(\nu)$ ($\nu = X, L$); and $E_x(\Gamma)$ is energy of the valence-band maximum. With the above twelve relations, we are left with seven independent parameters. We note that U_{sx} and W_{sx} do not enter in the previous relations; thus, they can be adjusted independently to fine tune the light-hole band effective masses in both $[001]$ and $[111]$ directions.

- ¹L. L. Chang, L. Esaki, and R. Tsu, *Appl. Phys. Lett.* **24**, 593 (1974).
- ²W. D. Goodhue, T. C. L. G. Sollner, H. Q. Le, E. R. Brown, and B. A. Vojak, *Appl. Phys. Lett.* **49**, 1086 (1986).
- ³L. F. Luo, R. Beresford, W. I. Wang, and E. E. Mendez, *Appl. Phys. Lett.* **54**, 2133 (1989).
- ⁴A. R. Bonnefoi, T. C. McGill, and R. D. Burnham, *Phys. Rev. B* **37**, 8754 (1987).
- ⁵Timothy B. Boykin, Jan P. A. van der Wagt, and James S. Harris, Jr., *Phys. Rev. B* **43**, 4777 (1990).
- ⁶M. K. Jackson, D. Z.-Y. Ting, D. H. Chow, D. A. Collins, J. R. Söderström, and T. C. McGill, *Phys. Rev. B* **43**, 4856 (1990).
- ⁷D. Z.-Y. Ting and T. C. McGill, *Phys. Rev. B* **47**, 7281 (1993).
- ⁸J. C. Chiang and Jiann-Shing Shyu, *Appl. Phys. Lett.* **70**, 2174 (1997).
- ⁹E. R. Brown, in *Hot Carriers in Semiconductor Nanostructures: Resonant Tunneling in High-speed Double-barrier Diodes*, edited by Jagdeep Shan (Academic, New York, 1992), pp. 469–496.
- ¹⁰E. R. Brown, W. D. Goodhue, and T. C. L. G. Sollner, *J. Appl. Phys.* **64**, 1519 (1988).
- ¹¹D. Z.-Y. Ting and J. N. Schulman, *Phys. Rev. B* **45**, 3583 (1992).
- ¹²Tom P. E. Broekaert, Wai Lee, and Clifton G. Fonstad, *Appl. Phys. Lett.* **53**, 1545 (1988).
- ¹³J. C. Chiang and Y. C. Chang, *J. Appl. Phys.* **73**, 2402 (1993).
- ¹⁴Y. C. Chang and J. N. Schulman, *Phys. Rev. B* **25**, 3975 (1982).
- ¹⁵C. B. Duke, *Solid State Physics* (Academic, New York, 1969), Suppl. 10.
- ¹⁶*Numerical Data and Functional Relationships in Science and Technology*, edited by K.-H. Hellwege, Landolt-Börnstein, New Series, Group III, Vol. 17, Pt. a (Springer, Berlin, 1982); *Numerical Data and Functional Relationships in Science and Technology*, edited by K.-H. Hellwege, Landolt-Börnstein, Group III-IV, Vol. 22, Pt. a (Springer, Berlin, 1986).
- ¹⁷J. C. Chiang, *Appl. Phys. Lett.* **64**, 1956 (1994).
- ¹⁸J. C. Chiang, *Appl. Phys. Lett.* **65**, 2821 (1994).
- ¹⁹J. C. Chiang and W. C. Kuo, *Phys. Rev. B* **48**, 8040 (1993).
- ²⁰Jean-Marc Jancu, Reinhard Scholz, Fabio Beltram, and Franco Bassani, *Phys. Rev. B* **57**, 6493 (1998).